ADVANCED MATERIALS TECHNOLOGIES
www.advmattechnol.de

Plant-Based Substrate Materials for Flexible Green Electronics

Youngkyu Hwang, Min Ku Kim, Ze Zhao, Bongjoong Kim, Taehoo Chang, Teng Fei Fan, Mohammed Shahrudin Ibrahim, Subra Suresh, Chi Hwan Lee,* and Nam-Joon Cho**

With the increasing use of soft and flexible electronics, there is a growing need to develop substrate materials that mitigate potential environmental risks associated with non-degradable electronics waste from synthetic substrate materials. To address this issue, the authors develop a novel, 2D plant-based substrate termed "sporosubstrate", which is made of non-allergenic natural pollen. The pollen particle has a double-layered architecture with an ultra-tough sporopollenin exine, and a soft cellulose intine is engineered through an eco-friendly process. In this manner, a readily available, economical, biodegradable, and biocompatible microgel can be prepared. This microgel can be used to create a variety of flexible shapes with customized mechanical, geometrical, electronic, and functional properties and performance characteristics such as thermal, chemical, and mechanical stability and optical transparency. Moreover, the authors demonstrate here different applications of the flexible natural substrate made of pollen microgel for use in electronic devices for health monitoring and wearable wireless heating. The results of this work point to opportunities for the development of a new class of flexible green electronics based on plant-based materials in applications such as wearable sensors, implantable devices, and soft robotics.

1. Introduction

The development of ultrathin, portable, and flexible electronic devices and components has catalyzed rapid technological advances across a wide range of domains, including medicine,[1] telecommunication,[2] energy,[3] and robotics.[4] Synthetic polymers such as polyimide (PI),[5] polystyrene,[6] polypropylene,[7] and polyethylene terephthalate (PET)[8,9] are widely used as substrate materials in applications that incorporate transistors,[10] light-emitting diodes,[11] biosensors,[12,13] and organic photovoltaics.[14] However, the use of these chemically processed synthetic polymers, which are non-degradable, can lead to environmental degradation on land and in oceans. Consequently, the development and deployment of materials derived from abundant natural resources that are sustainable, eco-friendly, biocompatible, and biodegradable are receiving increasing attention.

Researchers have explored materials such as chitin,[15,16] nanocellulose,[17] and silk[18] as substrate materials to replace synthetic chemicals in electronics applications. For example, chitin, a fibrous material, has been considered a candidate substrate material for organic light-emitting diodes (OLEDs),[15] glucose sensors,[19] and heaters[19,20] owing to its robustness, non-toxicity, and biocompatibility. In addition, nanocellulose-based substrates with a low surface roughness, high transparency, and high elastic modulus (E = 6–17 GPa)[21,22] have been

Y. Hwang, Z. Zhao, T. F. Fan, M. S. Ibrahim, S. Suresh, N.-J. Cho
School of Materials Science and Engineering
Nanyang Technological University
50 Nanyang Avenue, Singapore 639798, Singapore
E-mail: ssuresh@ntu.edu.sg; njcho@ntu.edu.sg

Y. Hwang
School of Chemical Engineering and Translational
Nanobioscience Research Center
Sungkyunkwan University
Suwon 16419, Republic of Korea

M. K. Kim, B. Kim, C. H. Lee
Weldon School of Biomedical Engineering
Purdue University
West Lafayette, IN 47907, USA
E-mail: lee2270@purdue.edu

The ORCID identification number(s) for the author(s) of this article can be found under https://doi.org/10.1002/admt.202200446.

DOI: 10.1002/admt.202200446

M. K. Kim
School of Mechanical Engineering
Hanyang University
Seoul 04763, South Korea

B. Kim
Department of Mechanical and System Design Engineering
Hongik University
Seoul 04066, South Korea

T. Chang, C. H. Lee
School of Materials Engineering
Purdue University
West Lafayette, IN 47907, USA

C. H. Lee
School of Mechanical Engineering
Purdue University
West Lafayette, IN 47907, USA

C. H. Lee
School of Materials Engineering
Department of Speech
Language and Hearing Sciences
Purdue University
West Lafayette, IN 47907, USA

developed for use in energy storage devices,[23,24] OLEDs,[25] and organic photovoltaics.[26] Notably, the extraction of chitin and cellulose from diverse sources such as crabs,[27] wood,[26,28] algae,[29] and bacteria[5,23,25] is challenging in terms of the high extraction costs, low yield, and considerable processing time. Silk-based substrates exhibit high mechanical strength (E = 5–12 GPa)[30] and can be conveniently fabricated in large volumes. However, despite its excellent biocompatibility and biodegradability, silk is highly soluble in water, which limits its long-term reliable use in flexible and stretchable electronics.[5]

To overcome the foregoing limitations of the current alternatives to synthetic materials, we consider the feasibility of using plant-based substrates derived from plant pollen (termed "sporosubstrate") for application in flexible and stretchable electronics. Pollen is primarily composed of structural proteins, lipids, and sporopollenin in the exine (outer layer), and cellulose, hemicellulose, and pectin in the intine (inner layer).[31–34] Sporopollenin has high strength and can protect cellular materials from harsh environmental conditions such as high or low temperatures or exposure to acidic or alkaline solvents.[34] Considering its practically indestructible structural characteristics, sporopollenin has been studied as a candidate material for several applications such as micromotors and drug delivery systems.[19,35] Recently, we reported a process to transform hard pollen into a non-allergenic soft microgel, which can facilitate the design of a wide variety of natural and environmentally sustainable materials.[36–38] This unique process uses a pollen-based soft microgel as the building block for natural materials with tunable mechanical, physical, and functional properties.[39–42]

In this study, we demonstrate the feasibility of fabricating and deploying pollen-based materials as unique natural biopolymer substrates for flexible and stretchable electronics. By treating natural pollen with potassium hydroxide (KOH), cellular materials including lipids and proteins can be eliminated, and the hard pollen can be transformed into a non-allergenic, hollow, and soft microgel.[36] These sporopollenin particles then serve as building blocks to design stimuli responsive and flat-surfaced structures such as paper and cardboard,[43] and structures with complex shapes.[39] In particular, we tailor the mechanical, thermal, and chemical properties of the sporosubstrates for long-term reliable use in conventional devices. Moreover, we also highlight the feasibility of fabricating skin-mountable, stretchable physiological sensors and heaters on the sporosubstrate by using widely used processing methods such as laser-cutting, direct ink writing, and transfer printing to demonstrate the application potential of sporosubstrates in the broad domain of wearable biomedical devices.

2. Results and Discussion

The fabrication of a 2D substrate comprising pollen particles from the genus *Camellia* is schematically illustrated in Figure S1, Supporting Information. To decrease the surface roughness of the substrate, we selected *Camellia* pollen as its surface is smoother than that of other pollen plants such as sunflowers and *Lycopodium* (**Figure 1**a and Figure S2a, Supporting Information). Furthermore, the Young's modulus (E = 17.8 GPa) of *Camellia* pollen is similar to that of sunflowers (21.5 GPa) and *Lycopodium* (18.3 GPa) after defatting (Figure S2b, Supporting Information).

The small particles (<10 μm), lipids, and proteins that cause allergic reactions to pollen were removed[44–46] during defatting and subsequent treatment with KOH, as indicated by the Fourier-transform infrared (FT-IR) spectroscopic analysis (Figure S3, Supporting Information).[47,48] The resulting sporopollenin particles were spherical with apertures and pores, and the particles enclosed the generative cell (Figure 1b). The scanning electron microscope (SEM) image in Figure 1c shows that although the sporopollenin was flattened and hollow, it retained its strength after drying, and the unique structures of the exine and intine layers of sporopollenin were visible. Furthermore, the capillary forces induced by water evaporation both outside (i.e., between the pollen particles) and inside a pollen particle (i.e., between intines) facilitated the collapse and flattening of the sporopollenin layer (Figure 1e,f).[49,50] As the pollen particles underwent concomitant structural flattening, the carboxyl and hydroxyl functional groups on the surface of pollen components such as cellulose, pectate, and sporopollenin generated attractive forces, arising from van der Waals forces, electrostatic forces, and hydrogen bonding, to preserve the collapsed shape of pollen particles with tight particle–particle coupling.[51,52]

Next, we tailored the mechanical, chemical, and thermal properties of the sporosubstrate for the flexible electronics platform. The Young's modulus and tensile fracture strain were estimated to be 410 MPa and 37%, respectively, based on a uniaxial tensile test performed on a sporosubstrate pollen paper sheet. For commercial A4 paper (PaperOne, April Group), the corresponding values were 300 MPa and 12%, respectively (**Figure 2**a and Figure S4, Supporting Information). The sporosubstrate exhibited an approximately threefold higher tensile fracture strain to offer improved durability and reliability in performance particularly against deformations. To illustrate the deformability of the sporosubstrate and its amenability to being folded into complex shapes without cracking, we prepared origami arrangements in the shape of a crane, as shown in Figure 2b and Figure S5, Supporting Information. The sporosubstrate exhibited a higher chemical resistance to various solvents, such as deionized (DI) water, 2 M NaOH, 2 M HCl, and acetone, compared to polycarbonate (PC), PET, and PI films that are commonly used as substrates for flexible electronics (Figure 2c–f). According to mass measurements, the sporosubstrate exhibited a mass loss of 7.3%, 4.8%, 9.7%, and 2.7% in DI water, NaOH, HCl, and acetone after 7 days and there was no significant structural distortion even after 30 days in all of the tested solvents (Figure S6, Supporting Information).[53] On the other hand, the PI film fully dissolved in NaOH after only 12 h, and the PC film became brittle and opaque after being exposed to acetone for 6 h. To confirm the potential for applications using the materials, an electrode was formed on each substrate via 3D printing. In the case of PI and PC substrates, the electrode was disconnected within 1 day due to the dissolution and shape distortion of the substrates. Although the sporosubstrate showed a high resistance in NaOH after 2 days, it was caused by delamination of the electrode from the substrate (Figure S7, Supporting Information).

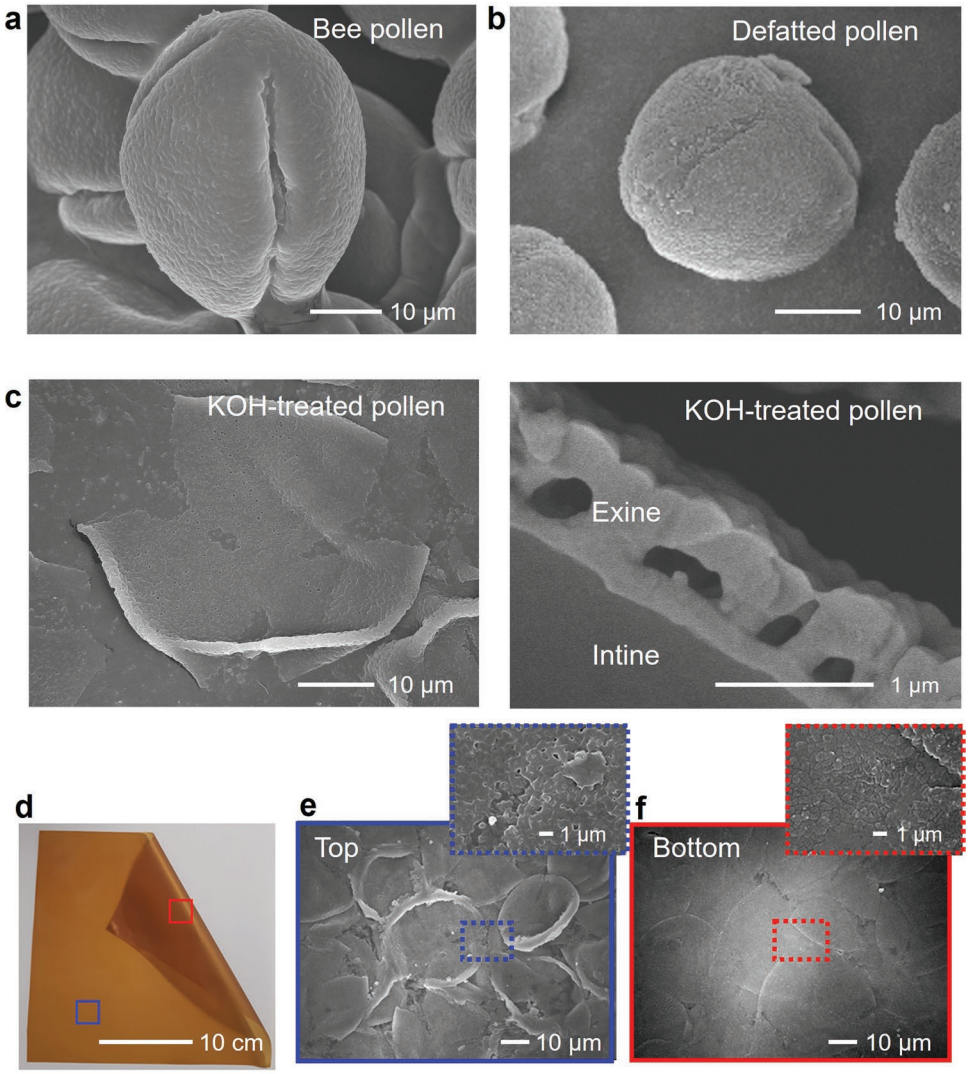

Figure 1. Fabrication and morphology of a sporosubstrate. SEM images of the a) bee pollen from *Camellia*, b) defatted pollen, and c) KOH-treated pollen. d) Photograph of the sporosubstrate. e,f) SEM images of the top and bottom side of a sporosubstrate corresponding to the representative sporosubstrate shown in Figure 1d. Inset images show the magnified SEM images of selected areas on the top and bottom sides of the sporosubstrate.

To evaluate the thermal stability of the sporosubstrate, we measured the change in its dimensions after heating at different temperatures (color): room temperature (RT, pale yellow), 100 (dark yellow), 200 (dark brown), and 250 °C (black) (Figure 2g). The decrease in the size of the sporosubstrate was small (3%) at 100 and 200 °C, and the chemical structure did not change significantly, as indicated by the FT-IR analysis (Figure S8a, Supporting Information). The thermogravimetric analysis (TGA) indicated that negligible weight change occurred at the temperature ranging from 110 to 210 °C (Figure S8b, Supporting Information).[54] In addition, the sporosubstrate showed 131×10^{-6} K^{-1} in ≈100–130 °C and 312×10^{-5} K^{-1} in ≈180–200 °C of the coefficient of linear thermal expansion (LCTE) (Figure S8c, Supporting Information). Although the thermal stability is relatively lower than other conventional substrates such as PI, PC, and PET, the sporosubstrate is stable up to a temperature of 210 °C.[55–57] Although the sporosubstrate exhibited a decrease in weight at 250 °C, it showed only 4% of a dimensional change and maintained rectangular shape due to high thermal resistance of the sporopollenin biopolymer. The results suggest that the sporosubstrate can maintain its structural properties, shape, and chemical composition, even at operating temperatures that exceed the typical service conditions for electronic devices.

To demonstrate the suitability of the sporosubstrate for flexible electronics, we designed and fabricated flexible electronics by adopting two widely used fabrication methods: indirect (transfer printing) and direct (patterning) methods. First, an electrophysiological (EP) sensor, consisting of reference, ground, and recording electrodes, was fabricated on the sporosubstrate through transfer printing (**Figure 3**a–d and Figure S9, Supporting Information). Spin-cast layers of polymethyl methacrylate (PMMA, 1 μm thick) and PI (1 μm thick) were placed on a glass surface. Electron beam deposition was performed to deposit metal layers of chromium (Cr, 5 nm thick) and gold (Au, 150 nm thick), followed by standard photolithographic

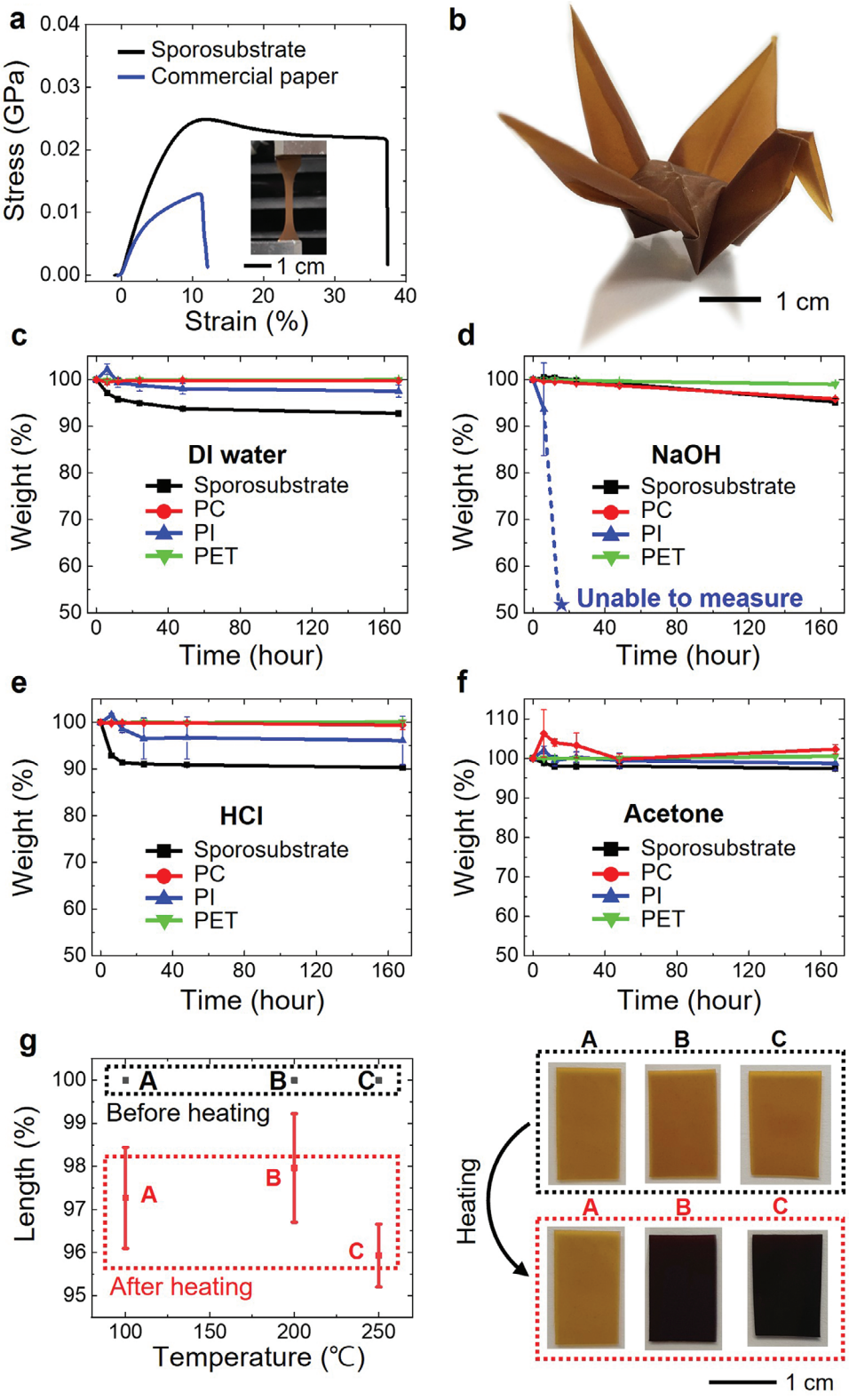

Figure 2. Characterization of the sporosubstrate. a) Strain–stress curve of the sporosubstrate. The inset image shows the sporosubstrate mechanically deformed in tension. b) Photograph of the crane origami form prepared using the sporosubstrate. c–f) Weight of the sporosubstrate in various solvents (2 M NaOH, 2 M HCl, acetone, and DI water) with different incubation times (6, 12, 24, 48, and 168 h) at room temperature (22 °C, $n = 3$). g) Length of the heat-treated sporosubstrate. Photographs in dotted boxes show the sporosubstrate before (black) and after (red) heat treatment at 100, 200, and 250 °C for 30 min ($n = 3$).

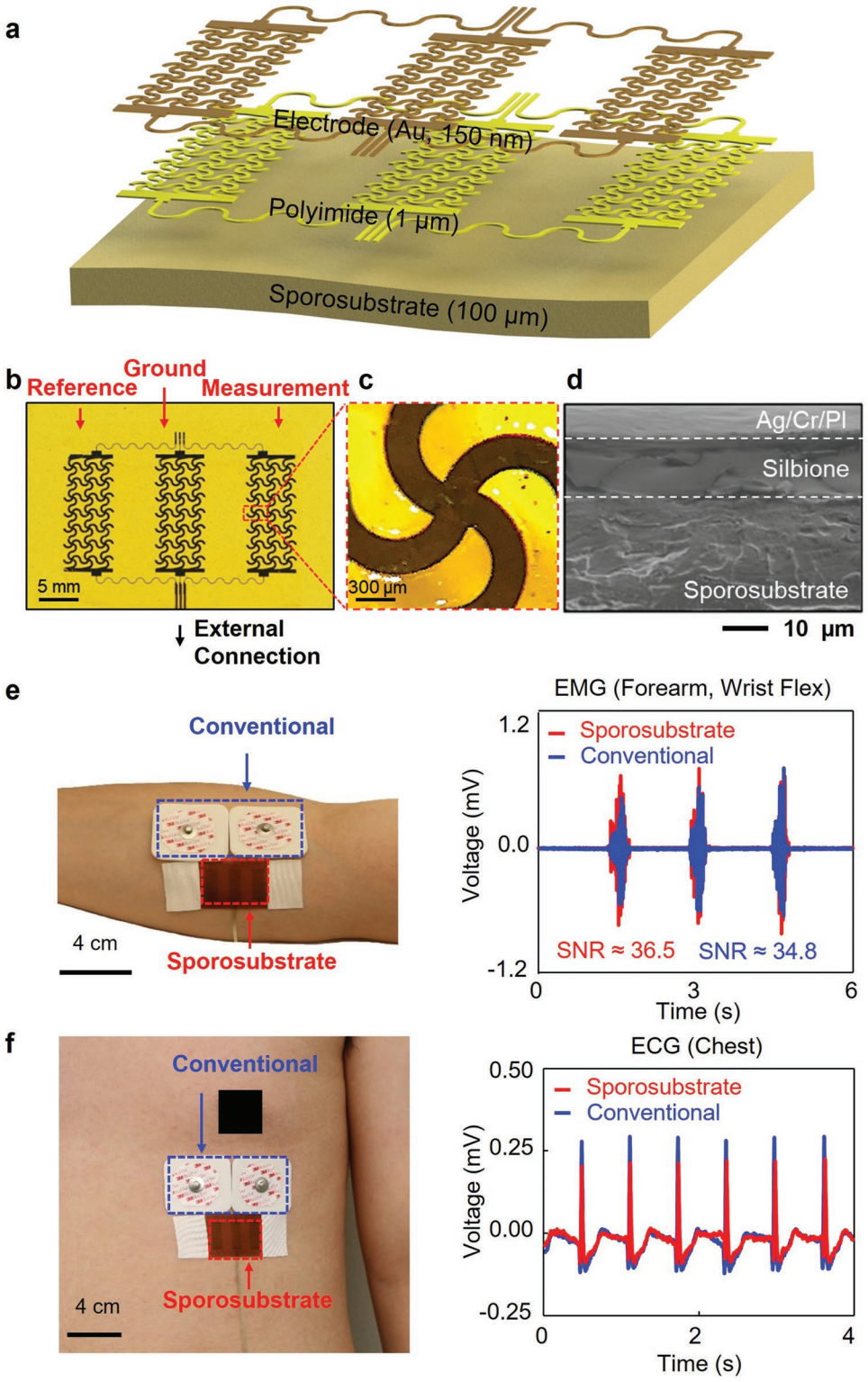

Figure 3. Electrophysiological (EP) sensor application of the sporosubstrate. a) Schematic of EP sensor built on the sporosubstrate. b,c) Photograph and microscopy images of the EP sensor. d) Cross-sectional SEM image highlighting the interfacial layers within the EP sensor. e,f) Photographs (left) and measurement results (right) of the EP sensor in contact with the forearm skin and chest, respectively.

patterning to create a stretchable form (i.e., filamentary serpentine mesh). The entire structure was immersed in acetone to eliminate the PMMA layer, allowing the thin film metal layer to be released from the glass and transferred onto the sporosubstrate using medical-grade silicone adhesive with high water and gas permeability, which also acts as an adhesive when attaching the electrode to the skin during EP recording. High-fidelity recordings of electromyogram (EMG) and electrocardiogram (ECG) signals were obtained by attaching the sporosubstrate-based sensor on the right forearm (Figure 3e) and chest (Figure 3f) of a healthy adult. The results were similar to those simultaneously obtained using conventional EP recording electrodes. This is also demonstrated by the impedance measurement across the two electrodes attached to the skin of the forearm area (Figure S10, Supporting Information). Moreover, no skin irritation or discomfort was noticed following >30 min of the use. The EMG signals acquired during three consecutive wrist flexes exhibited comparable signal-to-noise ratios (sporosubstrate: 36.5, conventional: 34.8), baseline noise levels (sporosubstrate: 1.79 μV, conventional: 1.92 μV), and a Pearson correlation coefficient (r)—which indicates the statistical association between the two signals—of 85%. Notably, the ECG signals exhibited a high r value of ≈98% demonstrating a strong correlation between recorded signals and were indicative of a P-wave (atrial depolarization), a QRS-complex (ventricular depolarization), and a T-wave (ventricular repolarization) (Figure S11, Supporting Information).

Next, a skin-mountable heating patch was prepared (**Figure 4**a,b). The sporosubstrate was successfully patterned into a stretchable Joule heating configuration using a laser cutter that induced no thermal damage or distortion, as indicated in the optical images (Figure S12, Supporting Information). Next, AgTPU ink (thermoplastic polyurethane with Ag flakes) and polydimethylsiloxane (PDMS) were directly printed onto the sporosubstrate (Figure S13, Supporting Information).[58] The water vapor transmission rate of sporosubstrate was 0.09 g cm^{-2} day^{-1} compared to the 0.27 g cm^{-2} day^{-1} of open bottle, and the open mesh design of the heating patch (≈60% open area) allows oxygen and water vapor transmission permeability through the open mesh area for skin breathability and minimizes the effect of sweat on the sporosubstrate (Figure S14, Supporting Information). It also enables stretchability and conformal contact with the curvature of skin through deformation in flexure. To characterize the resulting heating patch, we measured the relative change in the resistance which is the ratio of the instantaneous resistance to the resistance at zero strain, R/R_0, of the heating patch at uniaxial stretching of up to 65% (Figure 4c). The R/R_0 remained constant (less than 1.5) until an elongation strain of up to ≈40% and then abruptly increased until it reached the limit at ≈65%. The R/R_0 remained at 3 and 5 for more than 1000 cycles of stretching at the applied strain of up to 30% and 40%, respectively (Figure S15, Supporting Information). Figure 4d shows the experimental results obtained from the heating patch (3 cm × 2 cm) by applying input voltages of 0.5, 0.75, and 1.0 V for 120 s each with an external power source to reach the target temperature at ≈31, ≈38, and ≈45 °C, respectively. For comparison, the same heating patch was also printed on PI (80 μm thick) and PET (65 μm thick) substrates, which showed negligible differences in the target temperature (i.e. <0.67 °C) (Figure S16, Supporting Information). The results of finite element analysis (FEA) modeling complemented these findings and indicated local maximum principal strains (ε_{max}) of <6% across the entire surface of the heating patch under stretching at the applied strain up to 40% (Figure 4e).

Articular thermotherapy is often practiced to alleviate joint pain and stiffness by inducing vasodilation to promote blood flow to the target area.[59] To achieve therapeutic results, conformal contact with the skin must be ensured to realize efficient heat transfer and precise temperature control (≈40 °C).[60] To demonstrate this, the heating patch was applied on the wrist of a human subject. A custom-made portable wristwatch was wired to the heating patch as a control unit that could maintain the temperature at less than 45 °C to avoid any risk of skin burn (**Figure 5**a,b). The wristwatch included the following key components: 1) a 10 kΩ thermistor for temperature measurement; 2) an OLED to display the measured temperature; 3) a microcontroller for the control unit; 4) button switches for user controls (i.e., display/temperature settings and power on/off functions); and 5) a lithium-ion battery as the power source (Figure S17, Supporting Information). Figure 5c shows a representative infrared (IR) image of the heating patch that was controlled by the wristwatch at the set temperature of 42 °C. The wristwatch was also used to apply a pre-programmed heating cycle (e.g., 5 min on and 1 min off) for slightly under 1 h at the applied voltage of 1.0 V (Figure 5d).

3. Conclusion

In summary, we demonstrated a pollen-based sporosubstrate for its use in flexible and stretchable electronics. The sporosubstrate enabled compelling advantages over conventional synthetic plastics in terms of natural sourcing, environmental degradation, and sustainable processing. Various analyses were performed to characterize the sporosubstrate in terms of its physical, chemical, and thermal stability under appropriate practical conditions of intended applications. As proofs of concept, we successfully developed skin-mountable stretchable EP sensor and heating patch on the sporosubstrate by using indirect and direct fabrication approaches. Although the sporosubstrate requires the further study to improve its properties such as relatively low transmittance and high LCTE compared to other biopolymer based materials, the sporosubstrate has strong potentiality as an ideal platform for a broad range of applications such as wearable biomedical devices, flexible/stretchable electronics, and soft robotics, and represents a low-cost and scalable solution to alternate the synthetic polymers across electronic sensor applications.

4. Experimental Section

Preparation of the Sporosubstrate: 1) Defatting: to produce defatted *Camellia* pollen particles, 250 g of natural bee pollen granules (Xi'an Yuenum Biological Technology Company Ltd., Shannxi Xian, China) were refluxed with 500 mL of acetone (Sigma-Aldrich) in

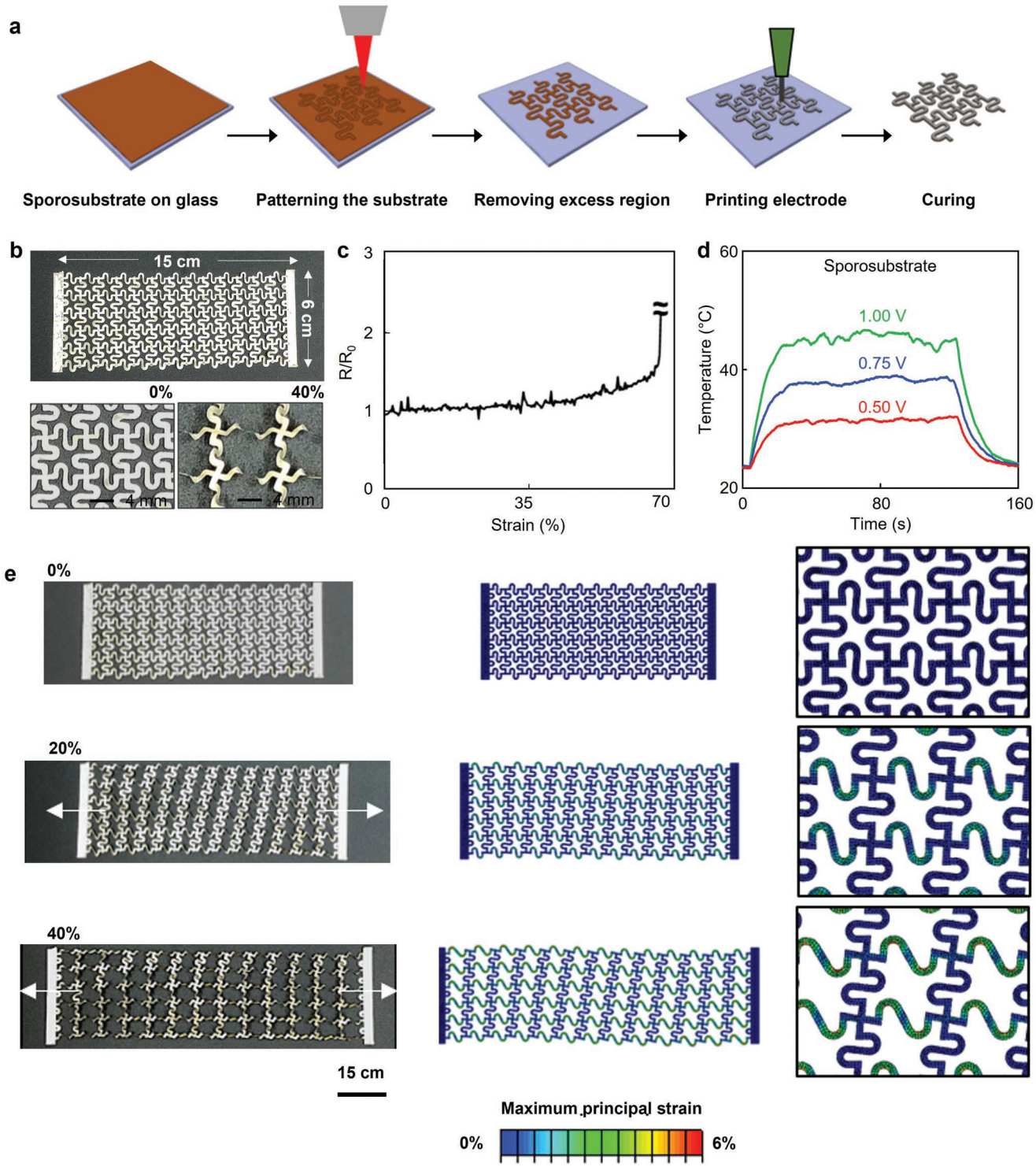

Figure 4. Stretchable heating patch on the sporosubstrate. a) Schematic of basic steps involved in the fabrication of a stretchable heating patch on the sporosubstrate. b) Photograph of the heating patch. The magnified images correspond to the heating patch under stretching at the applied strain of 0% and 40%. c) Normalized resistance versus strain curve of the heating patch. d) Temperature profiles of the heating patch at the applied voltages of 0.5 (red line), 0.75 (blue line), and 1 V (green line). e) Photograph and the corresponding FEA results of the heating patch under stretching at the applied strain up to 40%.

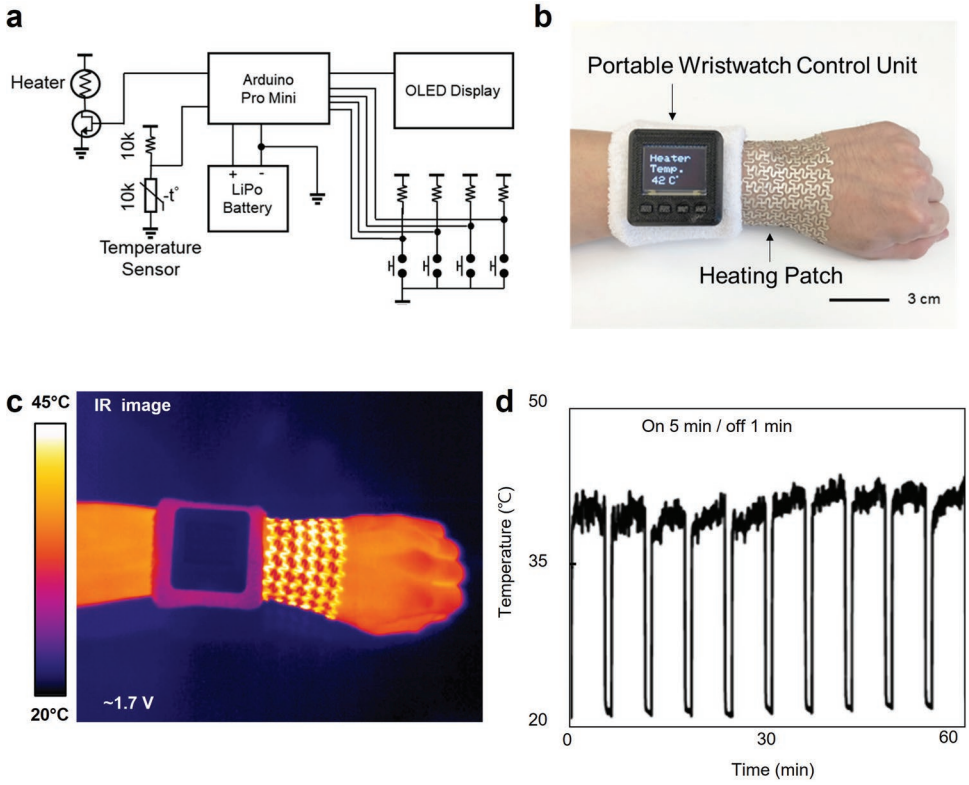

Figure 5. Application of the stretchable heating patch in Articular thermotherapy. a) Schematic of the circuitry embedded in the wristwatch control unit. b) Photograph of the heating patch connected to a custom-made wristwatch control unit on the wrist. c) IR image of (b) at an applied voltage of 1.7 V. d) Temperature profile of the heating patch under repeated on/off cycles.

a round-bottom flask (1 L) under stirring (200 rpm, IKA RCT) at 50 °C for 3 h. After stirring the pollen granules at 50 °C for 1 h with 1 L of deionized (DI) water (Direct-Q Water Purification System, Merck), the pollen solution was sequentially filtered using a nylon mesh (ELKO Filtering Co., diameter = 10 µm) and filter paper (diameter = 6 µm, Whatman) to remove the contaminant. The pollen particles were refluxed in 500 mL of acetone while stirring at 50 °C for 3 h. Subsequently, the particles were subjected to vacuum filtration and dried for 12 h in a fume hood to remove acetone residues. Next, 20 g of dried pollen powder was refluxed with 250 mL of diethyl ether (Sigma-Aldrich) while stirring at 25 °C for 2 h, followed by two cycles of vacuum filtration to remove the low-polarity fat compound. Finally, the pollen solution, after stirring with diethyl ether at 25 °C for 12 h, was filtrated and dried for 12 h in a fume hood; and 2) cytoplasm removal: after refluxing the defatted pollen with 200 mL of potassium hydroxide (KOH) solution (Sigma-Aldrich, 10 wt% in DI water) while stirring at 80 °C for 2 h in a round-bottom flask, the suspension was transferred to a conical tube and centrifuged to remove the KOH solution. In the suspension, 40 mL of fresh KOH solution (10 wt%) was added, and the resuspended pollen particles were centrifuged to remove the residues (4500 rpm, 5 min, Allegra X-15R, Beckman Coulter, Inc.). After discarding the supernatant, the pollen particles were collected in a beaker (1 L) with 300 mL of DI water (50 °C). After incubating the particles while stirring for 5 min, five cycles of filtration were performed using a nylon mesh (pore size = 10 µm) to neutralize the pollen solution to a pH level of 7–7.5.

FT-IR Spectroscopy and TGA Measurement: Chemical analysis was conducted via FT-IR spectroscopy (Frontier, PerkinElmer) with a diamond cell attenuated total reflection accessory module. Transmittance was obtained using an ultraviolet–visible (UV–Vis) spectrometer (UV-2700, SHIMADZU) and thermal analysis was conducted using a Q500 instrument (TA Instruments).

Sample Imaging: Optical micrograph and SEM images were obtained using a Nikon TS100 and a JSM-7600F Schottky field-emission scanning electron microscope (JEOL), respectively. A Park XE-100 device was used to obtain atomic force microscopy (AFM) images (non-contact mode, scan area = 20 µm × 20 µm, scan rate = 0.2–0.5 Hz, NX-10, Park Systems) at RT by using an aluminum reflex-coated silicon cantilever, PPP-NCHR (spring constant ≈42 N m^{-1}, Nanosensors).

Young's Modulus Measurement: To measure the Young's modulus through the AFM technique, a gold reflex-coated silicon cantilever, biosphere B2000-NCH (diameter = 4 µm, spring constant ≈40 N m^{-1}, Nanotools, Germany), was used to obtain the force–displacement (FD) curve from 16 points of the selected area in the sporosubstrate (lateral dimension = 10 µm × 10 µm, approach speed = 0.8 µm s^{-1}, and maximum loading force = 6.0 µN). To remove the contaminants, the AFM cantilever was rinsed with water and ethanol, followed by UV cleaning for 30 min. To calculate Young's modulus, the Hertzian model was used for curve fitting in XEI (Park Systems) and Python. The authors determined Young's modulus from the FD curve according to the equation:

$$F = \frac{E}{1-\nu^2}\left[\frac{a^2+R^2}{2}\ln\frac{R+a}{R-a} - aR\right], \delta = \frac{a}{2}\ln\frac{R+a}{R-a} \quad (1)$$

where E is Young's modulus, ν is Poisson's ratio, a is the contact radius, R is the radius of the sphere, and δ is the indentation depth. ν was set as 0.5, which is a typical value for biological materials.

Mechanical Tensile Test: A tensile test was performed using electromechanical universal test systems (MTS 42, MTS Systems Corporation), and the tensile speed was 1 cm min^{-1} at RT under ≈60–70% of humidity. The sample was prepared using a dumbbell-shaped cutter (dimension of the center = 7.6 mm × 3.2 mm, SDL-100, DUMBBELL CO., LTD.). The thickness and weight were measured using a micrometer (MDC-25PX, Mitutoyo Asia Pacific Pte Ltd.) and

analytical weighing balance (BBX 22, BOECO, Germany), respectively. Moreover, a resistance–strain test was conducted using a dynamic mechanical analyzer (ESM303, Mark-10 Corp.) and source measure unit (Keithley 2400, Tektronix, Inc.). The temperature was measured using an IR camera (SC645, FLIR Systems, Inc.). The LCTE was measured by standard test methods for linear thermal expansion of solid materials by thermomechanical analysis in ≈30–200 °C of the temperature range (5 °C min^{-1}, ASTEM E831, TA instrument, USA).

Fabrication of the Electrophysiological Sensor: Successive layers of PMMA (thickness = 1 μm) and PI (thickness = 1 μm) were spin-coated on a glass substrate. An electron beam evaporator was used to deposit subsequent layers of Cr/Au (5 nm/150 nm). Standard photolithographic patterning with a photoresist (AZ 1518, 3000 rpm, 30 s) and wet etching with Cr and Au etchant (Transene, Inc.) were conducted, followed by oxygen plasma reactive-ion etching, to define the filamentary serpentine patterns for the EP electrodes. The resulting structure was immersed in acetone for 1 h to dissolve the bottom PMMA layer and release the remaining thin films from the glass substrate. The released thin films were transferred to a pre-formed sporosubstrate and glued using a thin layer (<10 μm thick) of a medical-grade silicone adhesive (Silbione, RT GEL 4317, Elkem Silicones). The schematics of these steps are shown in Figure S9, Supporting Information.

Preparation of the Ag flake/PU Ink: Ag flake/PU ink was prepared by first dissolving 1.48 g of PU (Elastollan Soft 35A, BASF) in a solution of 1.56 mL of *N*,*N*-dimethylformamide (DMF) (Sigma-Aldrich) and 4.27 mL of tetrahydrofuran (THF) (Sigma-Aldrich). Next, 5.92 g of Ag flakes (99.95%, average particle size [APS] 2–5 μm; 47MR-10F, Inframat Advanced Materials) was mixed in a planetary mixer (ARE-310, Thinky U.S.A., Inc.) for 10 min at 2000 rpm. The resulting mixture was loaded into a 3 cc syringe (Nordson EFD) and centrifuged at 2500 rpm for 2 min to remove the air bubbles trapped in the mixture.

Fabrication of the Stretchable Heating Patch: First, a pre-formed sporosubstrate was mounted on a glass substrate. A high-precision laser cutter (PLS6MW, Universal Laser systems, 15 W CO_2 laser, $\lambda = 10.6$ μm, spot size = 130 μm and spatial resolution = 25.4 μm) was used to pattern an outline of the Joule heating element. Conduction paths were printed on the surface by extruding the Ag flake/PU ink by using a three-axis automated fluid dispensing robot (PRO4, Nordson EFD) and digital pneumatic regulator (Ultimus V High-Precision Dispenser, Nordson EFD). The printed Ag flake/PU layer was cured in a vacuum oven at 50 °C for 4 h, followed by automated dispensing of PDMS to form an encapsulation layer. The schematics of these steps are shown in Figure 4a. The external power source was a DP832 device (Rigol).

Recording of EP Signals from the Skin: The EP sensor was attached to the forearm skin and chest of a volunteer (age: 30 y) to capture the EMG and ECG signals, respectively. Before attaching the electrodes to the skin, an electrolyte gel (Signagel, Parker laboratories Inc.) was applied to enhance electrical impedance between the electrode and the skin. The generated EP signals were recorded using a preamplifier and data acquisition unit (Octal Bio Amp and Power Lab, ADInstruments) and transmitted to an external computing system. A commercial software (LabChart, ADInstruments) was used to process the collected data with a 60 Hz notch filter with a bandpass filter admitting frequencies of 10–500 and 0.5–100 Hz for the EMG and ECG signals, respectively. The conventional EP recording electrodes were RedDot (3M).

Numerical Simulation: The deformations of the sporosubstrate, Ag flake/PU, and PDMS were modeled by linear elastic behavior with the effective mechanical modulus (E) being 410 MPa, 60.8 GPa, and 1.84 MPa, respectively. The rule of mixtures was used to calculate the elastic modulus of Ag flake/PU ink (80% Ag and 20% PU). The entities were modeled using an eight-node brick element with reduced integration (C3D8R) solid elements. Displacement boundary conditions were applied to both edges of the structure to produce uniaxial tension for strains of 10%, 20%, 30%, and 40%.

Water Vapor Transmission Measurement: The petri dish (diameter: 1.3 mm) that contained DI water (4 mL) were covered by sporosubstrate and measured weight loss at room temperature under ≈24–30% humidity. As a comparison, the petri dish without cover was measured at the same time.

Statistical Analysis: The quantitative values in this study are presented as means ± standard deviation. The quantitative experiments were conducted with three replicates. The size change of samples was measured by ImageJ software (National Institutes of Health, Bethesda, MD). All participants provided written, informed consent prior to participation in the study.

Supporting Information

Supporting Information is available from the Wiley Online Library or from the author.

Acknowledgements

Y.H. and M.K.K. contributed equally to this work. This work was supported by the National Research Foundation of Singapore through a Competitive Research Programme grant (NRF-CRP10-2012-07) and by the Ministry of Education of Singapore through a AcRF Tier 1 grant 2017-T1-001-246 (RG51/17). This work was also supported by the SKKU Research Fellowship Program of Sungkyunkwan University, 2022 and by the Basic Science Research Program through the National Research Foundation of Korea (NRF) funded by the Ministry of Education (2021R1I1A1A01056302). C.H.L. acknowledges the National Science Foundation (NSF) Chemical, Bioengineering, Environment, and Transport Systems (CBET) (Award Number: 2032529).

Conflict of Interest

The authors declare no conflict of interest.

Data Availability Statement

Research data are not shared.

Keywords

biological materials, biopolymers, flexible electronics, pollen grains, wearable electronics

Received: April 6, 2022
Published online:

[1] R. C. Webb, A. P. Bonifas, A. Behnaz, Y. Zhang, K. J. Yu, H. Cheng, M. Shi, Z. Bian, Z. Liu, Y. S. Kim, W. H. Yeo, J. S. Park, J. Song, Y. Li, Y. Huang, A. M. Gorbach, J. A. Rogers, *Nat. Mater.* **2013**, *12*, 938.
[2] B. S. Kim, K. Y. Shin, J. B. Pyo, J. Lee, J. G. Son, S. S. Lee, J. H. Park, *ACS Appl. Mater. Interfaces* **2016**, *8*, 2582.
[3] B. N. Chandrashekar, B. Deng, A. S. Smitha, Y. Chen, C. Tan, H. Zhang, H. Peng, Z. Liu, *Adv. Mater.* **2015**, *27*, 5210.
[4] E. J. Markvicka, M. D. Bartlett, X. Huang, C. Majidi, *Nat. Mater.* **2018**, *17*, 618.
[5] D. H. Kim, J. Viventi, J. J. Amsden, J. Xiao, L. Vigeland, Y. S. Kim, J. A. Blanco, B. Panilaitis, E. S. Frechette, D. Contreras, D. L. Kaplan, F. G. Omenetto, Y. Huang, K. C. Hwang, M. R. Zakin, B. Litt, J. A. Rogers, *Nat. Mater.* **2010**, *9*, 511.

[6] X. Xiao, L. Yuan, J. Zhong, T. Ding, Y. Liu, Z. Cai, Y. Rong, H. Han, J. Zhou, Z. L. Wang, *Adv. Mater.* **2011**, *23*, 5440.
[7] G. A. Salvatore, N. Munzenrieder, T. Kinkeldei, L. Petti, C. Zysset, I. Strebel, L. Buthe, G. Troster, *Nat. Commun.* **2014**, *5*, 2982.
[8] H. Zhu, X. Wang, J. Liang, H. Lv, H. Tong, L. Ma, Y. Hu, G. Zhu, T. Zhang, Z. Tie, Z. Liu, Q. Li, L. Chen, J. Liu, Z. Jin, *Adv. Funct. Mater.* **2017**, *27*, 1606604.
[9] H. Jang, Y. J. Park, X. Chen, T. Das, M. S. Kim, J. H. Ahn, *Adv. Mater.* **2016**, *28*, 4184.
[10] T. Someya, Y. Kato, T. Sekitani, S. Iba, Y. Noguchi, Y. Murase, H. Kawaguchi, T. Sakurai, *Proc. Natl. Acad. Sci. USA* **2005**, *102*, 12321.
[11] J. Li, C. Zhang, L. Duan, L. M. Zhang, L. D. Wang, G. F. Dong, Z. L. Wang, *Adv. Mater.* **2016**, *28*, 106.
[12] Y. Yang, X. Yang, X. Zou, S. Wu, D. Wan, A. Cao, L. Liao, Q. Yuan, X. Duan, *Adv. Funct. Mater.* **2017**, *27*, 1604096.
[13] O. S. Kwon, S. J. Park, J. Y. Hong, A. R. Han, J. S. Lee, J. S. Lee, J. H. Oh, J. Jang, *ACS Nano* **2012**, *6*, 1486.
[14] M. Kaltenbrunner, G. Adam, E. D. Glowacki, M. Drack, R. Schwodiauer, L. Leonat, D. H. Apaydin, H. Groiss, M. C. Scharber, M. S. White, N. S. Sariciftci, S. Bauer, *Nat. Mater.* **2015**, *14*, 1032.
[15] J. Jin, D. Lee, H. G. Im, Y. C. Han, E. G. Jeong, M. Rolandi, K. C. Choi, B. S. Bae, *Adv. Mater.* **2016**, *28*, 5169.
[16] J. Huang, Y. Zhong, L. Zhang, J. Cai, *Adv. Funct. Mater.* **2017**, *27*, 1701100.
[17] T. Lei, M. Guan, J. Liu, H. C. Lin, R. Pfattner, L. Shaw, A. F. McGuire, T. C. Huang, L. Shao, K. T. Cheng, J. B. Tok, Z. Bao, *Proc. Natl. Acad. Sci. USA* **2017**, *114*, 5107.
[18] R. K. Pal, S. C. Kundu, V. K. Yadavalli, *ACS Appl. Mater. Interfaces* **2018**, *10*, 9620.
[19] H. Wang, M. G. Potroz, J. A. Jackman, B. Khezri, T. Marić, N.-J. Cho, M. Pumera, *Adv. Funct. Mater.* **2017**, *27*, 1702338.
[20] S. Ifuku, H. Saimoto, *Nanoscale* **2012**, *4*, 3308.
[21] H. Koga, M. Nogi, N. Komoda, T. T. Nge, T. Sugahara, K. Suganuma, *NPG Asia Mater.* **2014**, *6*, e93.
[22] D. Klemm, F. Kramer, S. Moritz, T. Lindstrom, M. Ankerfors, D. Gray, A. Dorris, *Angew. Chem., Int. Ed. Engl.* **2011**, *50*, 5438.
[23] S. Li, D. Huang, J. Yang, B. Zhang, X. Zhang, G. Yang, M. Wang, Y. Shen, *Nano Energy* **2014**, *9*, 309.
[24] J. Huang, H. Zhu, Y. Chen, C. Preston, K. Rohrbach, J. Cumings, L. Hu, *ACS Nano* **2013**, *7*, 2106.
[25] C. Legnani, C. Vilani, V. L. Calil, H. S. Barud, W. G. Quirino, C. A. Achete, S. J. L. Ribeiro, M. Cremona, *Thin Solid Films* **2008**, *517*, 1016.
[26] Z. Fang, H. Zhu, Y. Yuan, D. Ha, S. Zhu, C. Preston, Q. Chen, Y. Li, X. Han, S. Lee, G. Chen, T. Li, J. Munday, J. Huang, L. Hu, *Nano Lett.*. **2014**, *14*, 765.
[27] M. Rinaudo, *Prog. Polym. Sci.* **2006**, *31*, 603.
[28] H. Zhu, Z. Fang, Z. Wang, J. Dai, Y. Yao, F. Shen, C. Preston, W. Wu, P. Peng, N. Jang, Q. Yu, Z. Yu, L. Hu, *ACS Nano* **2016**, *10*, 1369.
[29] I. Tsekos, *J. Phycol.* **1999**, *35*, 635.
[30] C. Jiang, X. Wang, R. Gunawidjaja, Y. H. Lin, M. K. Gupta, D. L. Kaplan, R. R. Naik, V. V. Tsukruk, *Adv. Funct. Mater.* **2007**, *17*, 2229.
[31] J. M. Tylianakis, *Science* **2013**, *339*, 1532.
[32] D. Southworth, *J. Histochem. Cytochem.* **1973**, *21*, 73.
[33] T. D. Quilichini, E. Grienenberger, C. J. Douglas, *Phytochemistry* **2015**, *113*, 170.
[34] F. S. Li, P. Phyo, J. Jacobowitz, M. Hong, J. K. Weng, *Nat. Plants* **2019**, *5*, 41.
[35] R. C. Mundargi, M. G. Potroz, S. Park, H. Shirahama, J. H. Lee, J. Seo, N. J. Cho, *Small* **2016**, *12*, 1167.
[36] T. F. Fan, S. Park, Q. Shi, X. Zhang, Q. Liu, Y. Song, H. Chin, M. S. B. Ibrahim, N. Mokrzecka, Y. Yang, H. Li, J. Song, S. Suresh, N. J. Cho, *Nat. Commun.* **2020**, *11*, 1449.
[37] T. F. Fan, M. G. Potroz, E. L. Tan, M. S. Ibrahim, E. Miyako, N. J. Cho, *Sci. Rep.* **2019**, *9*, 9626.
[38] T.-F. Fan, Y. Hwang, M. G. Potroz, K.-L. Lau, E.-L. Tan, M. S. Ibrahim, E. Miyako, N.-J. Cho, *Appl. Mater. Today* **2020**, *19*, 100594.
[39] Z. Zhao, J. Kumar, Y. Hwang, J. Deng, M. S. B. Ibrahim, C. Huang, S. Suresh, N. J. Cho, *Proc. Natl. Acad. Sci. USA* **2021**, *118*, e2113715118.
[40] Y. Hwang, A. Sadhu, S. Shin, S. W. Leow, Z. Zhao, J. Deng, J. A. Jackman, M. Kim, L. H. Wong, N. J. Cho, *Adv. Mater.* **2021**, *33*, 2100566.
[41] S. Chen, Q. Shi, T. Jang, M. S. B. Ibrahim, J. Deng, G. Ferracci, W. S. Tan, N. J. Cho, J. Song, *Adv. Funct. Mater.* **2021**, *31*, 2106276.
[42] Y. Hwang, M. S. B. Ibrahim, J. Deng, J. A. Jackman, N. J. Cho, *Adv. Funct. Mater.* **2021**, *31*, 2101091.
[43] Z. Zhao, Y. Hwang, Y. Yang, T. Fan, J. Song, S. Suresh, N. J. Cho, *Proc. Natl. Acad. Sci. USA* **2020**, *117*, 8711.
[44] H. Yasueda, Y. Yui, T. Shimizu, T. Shida, *J. Allergy Clin. Immunol.* **1983**, *71*, 77.
[45] N. Prado, C. De Linares, M. L. Sanz, P. Gamboa, M. Villalba, R. Rodriguez, E. Batanero, *J. Immunol.* **2015**, *195*, 445.
[46] M. Grote, S. Vrtala, V. Niederberger, R. Valenta, R. Reichelt, *J. Allergy Clin. Immunol.* **2000**, *105*, 1140.
[47] E. L. Tan, M. G. Potroz, G. Ferracci, J. A. Jackman, H. Jung, L. L. Wang, N. J. Cho, *Adv. Funct. Mater.* **2018**, *28*, 1707568.
[48] M. Bagcioglu, B. Zimmermann, A. Kohler, *PLoS One* **2015**, *10*, e0137899.
[49] D. B. Asay, S. H. Kim, *J. Chem. Phys.* **2006**, *124*, 174712.
[50] M. Soleimani, R. J. Hill, T. G. M. van de Ven, *J. Mater. Sci.* **2015**, *50*, 5337.
[51] Y. Tian, N. Pesika, H. Zeng, K. Rosenberg, B. Zhao, P. McGuiggan, K. Autumn, J. Israelachvili, *Proc. Natl. Acad. Sci. USA* **2006**, *103*, 19320.
[52] M. K. Chaudhury, G. M. Whitesides, *Langmuir* **1991**, *7*, 1013.
[53] B. Fang, K. Pan, Q. Meng, B. Cao, *Polym. Int.* **2012**, *61*, 111.
[54] S. Bernard, K. Benzerara, O. Beyssac, E. Balan, G. E. Brown Jr., *Heliyon* **2015**, *1*, e00034.
[55] C. E. Sroog, *Prog. Polym. Sci.* **1991**, *16*, 561.
[56] W. Jiang, S. C. Tjong, *Polym. Degrad. Stab.* **1999**, *66*, 241.
[57] M. T. Freire, A. P. Damant, L. Castle, F. G. R. Reyes, *Packag. Technol. Sci.* **1999**, *12*, 29.
[58] A. D. Valentine, T. A. Busbee, J. W. Boley, J. R. Raney, A. Chortos, A. Kotikian, J. D. Berrigan, M. F. Durstock, J. A. Lewis, *Adv. Mater.* **2017**, *29*, 1703817.
[59] L. Brosseau, K. A. Yonge, V. Robinson, S. Marchand, M. Judd, G. Wells, P. Tugwell, *Cochrane Database Syst. Rev.* **2003**, *4*, CD002823.
[60] S. Choi, J. Park, W. Hyun, J. Kim, J. Kim, Y. B. Lee, C. Song, H. J. Hwang, J. H. Kim, T. Hyeon, D. H. Kim, *ACS Nano* **2015**, *9*, 6626.